Developmental stage-specific proliferation and retinoblastoma genesis in RB-deficient human but not mouse cone precursors

Hardeep P. Singh[a,b], Sijia Wang[a,b,c], Kevin Stachelek[a,b,d], Sunhye Lee[a,b], Mark W. Reid[a,b], Matthew E. Thornton[e], Cheryl Mae Craft[f,g], Brendan H. Grubbs[e], and David Cobrinik[a,b,c,f,h,i,1]

[a]The Vision Center, Children's Hospital Los Angeles, Los Angeles, CA 90027; [b]The Saban Research Institute, Children's Hospital Los Angeles, Los Angeles, CA 90027; [c]Cancer Biology and Genomics Program, Keck School of Medicine of the University of Southern California, Los Angeles, CA 90033; [d]Translational Biotechnology Program, Keck School of Medicine of the University of Southern California, Los Angeles, CA 90033; [e]Maternal-Fetal Medicine Division of the Department of Obstetrics and Gynecology, Keck School of Medicine of the University of Southern California, Los Angeles, CA 90033; [f]USC Roski Eye Institute, Department of Ophthalmology, Keck School of Medicine of the University of Southern California, Los Angeles, CA 90033; [g]Department of Integrative Anatomical Sciences, Keck School of Medicine of the University of Southern California, Los Angeles, CA 90033; [h]Department of Biochemistry and Molecular Medicine, Keck School of Medicine of the University of Southern California, Los Angeles, CA 90033; and [i]Norris Comprehensive Cancer Center, Keck School of Medicine of the University of Southern California, Los Angeles, CA 90033

Edited by Anton Berns, The Netherlands Cancer Institute, Amsterdam, The Netherlands, and approved August 15, 2018 (received for review May 23, 2018)

Most retinoblastomas initiate in response to the inactivation of the *RB1* gene and loss of functional RB protein. The tumors may form with few additional genomic changes and develop after a premalignant retinoma phase. Despite this seemingly straightforward etiology, mouse models have not recapitulated the genetic, cellular, and stage-specific features of human retinoblastoma genesis. For example, whereas human retinoblastomas appear to derive from cone photoreceptor precursors, current mouse models develop tumors that derive from other retinal cell types. To investigate the basis of the human cone-specific oncogenesis, we compared developmental stage-specific cone precursor responses to RB loss in human and murine retina cultures and in cone-specific *Rb1*-knockout mice. We report that RB-depleted maturing (ARR3$^+$) but not immature (ARR3$^-$) human cone precursors enter the cell cycle, proliferate, and form retinoblastoma-like lesions with Flexner–Wintersteiner rosettes, then form low or nonproliferative premalignant retinoma-like lesions with fleurettes and p16^{INK4A} and p130 expression, and finally form highly proliferative retinoblastoma-like masses. In contrast, in murine retina, only RB-depleted immature (Arr3$^-$) cone precursors entered the cell cycle, and they failed to progress from S to M phase. Moreover, whereas intrinsically highly expressed MDM2 and MYCN contribute to RB-depleted maturing (ARR3$^+$) human cone precursor proliferation, ectopic MDM2 and Mycn promoted only immature (Arr3$^-$) murine cone precursor cell-cycle entry. These findings demonstrate that developmental stage-specific as well as species- and cell type-specific features sensitize to *RB1* inactivation and reveal the human cone precursors' capacity to model retinoblastoma initiation, proliferation, premalignant arrest, and tumor growth.

retinoblastoma | cone photoreceptor | cancer cell of origin | genetically engineered mouse models | retinoma

Retinoblastoma is a pediatric retinal cancer that initiates in response to biallelic inactivation of *RB1* or *MYCN* amplification (MYCNA) in a susceptible retinal cell type (1). *RB1*-null retinoblastomas are far more common than the MYCNA variety and form either with two somatic *RB1* mutations or with one germline and one somatically inactivated *RB1* allele. Loss of functional RB protein in the cell of origin is thought to enable limited proliferation leading to premalignant retinomas, from which rare cells escape to form retinoblastoma tumors (2). Retinomas are found at the base of most retinoblastomas, display differentiated histology, and express the senescence markers p16^{INK4A} and p130. The mechanism of escape from the retinoma stage is currently unknown but may require few genomic changes beyond biallelic *RB1* loss (3, 4). Accurate modeling of retinoma formation and escape may provide opportunities to improve treatment and prevent tumorigenesis in genetically predisposed children. However, genetically engineered animal models have not recapitulated the genetic, cellular, and stage-specific features of human retinoma or retinoblastoma genesis.

In humans, germline *RB1*-null mutations predispose to retinoblastoma with ~90% penetrance (5). In contrast, mice with germline *Rb1* mutations (6–8) or chimeric biallelic *Rb1* loss (9, 10) fail to develop retinal tumors. Mouse retinal tumors can form when biallelic *Rb1* loss is combined with inactivation of *Rbl1* (encoding p107) (11–14), *Rbl2* (encoding p130) (15, 16), or *Cdkn1b* (encoding p27) (17) or when combined with Mycn overexpression (18). However, in contrast to the efficient development of human retinoblastoma from rare *RB1*$^{-/-}$ cells, murine retinal tumors formed only when millions of retinal cells had *Rb1* loss combined with other genetically engineered changes, suggesting that still further genomic changes were needed (16). Moreover, although the mouse tumors formed Homer–Wright rosettes, which are common to diverse neuronal tumors (19), they lacked retinoblastoma-specific Flexner–Wintersteiner rosettes and did not progress through a retinoma stage. Furthermore, the mouse tumors prominently expressed

Significance

Retinoblastoma is a childhood tumor that forms in response to mutations in the *RB1* gene and loss of functional RB protein. Prior studies suggested that retinoblastomas arise from cone photoreceptor precursors, whereas mouse models yield tumors deriving from other retinal cell types and lacking human retinoblastoma features. We show that in cultured human retinae, retinoblastomas initiate from RB-depleted cone precursors that are in a specific maturation state and form premalignant retinomas prior to retinoblastoma lesions, as is believed to occur in retinoblastoma patients. In contrast, Rb-deficient mouse cone precursors of similar maturation state and supplemented with human cone precursor-specific oncoproteins fail to proliferate. Thus, human species-specific developmental features underlie retinoblastoma genesis and may challenge the production of accurate retinoblastoma models.

Author contributions: H.P.S. and D.C. designed research; H.P.S., S.W., K.S., M.E.T., and D.C. performed research; S.L., C.M.C., and B.H.G. contributed new reagents/analytic tools; H.P.S., M.W.R., and D.C. analyzed data; and H.P.S. and D.C. wrote the paper.

The authors declare no conflict of interest.

This article is a PNAS Direct Submission.

[1]To whom correspondence should be addressed. Email: dcobrinik@chla.usc.edu.

This article contains supporting information online at www.pnas.org/lookup/suppl/doi:10.1073/pnas.1808903115/-/DCSupplemental.

Published online September 13, 2018.

retinal interneuron-specific proteins (11–15), whereas human retinoblastomas predominantly express cone photoreceptor proteins (20–24). Thus, current mouse models lack the cone protein expression, histologic features, and tumorigenesis stages of RB-deficient human retinoblastomas.

The different phenotypes of human retinoblastomas and mouse retinal tumors likely reflect their origins from different retinal cell types. Whereas it has been suggested that mouse retinal tumors possibly originate from retinal progenitor cells (14), from horizontal or amacrine interneurons (11, 25), or from a multipotent cell capable of producing amacrine and horizontal cells (16), human retinoblastomas appear to develop from postmitotic cone photoreceptor precursors (26, 27). Indeed, RB depletion enabled the proliferation of cone precursors but not of other retinal cells, and proliferation depended on transcription factors (RXRγ and TRβ2) and oncoproteins (MDM2 and MYCN) that are highly expressed during human cone maturation (24, 27). The cone precursors responding to RB loss also expressed maturation markers such as L/M-opsin and cone arrestin (ARR3) and formed tumors with retinoblastoma-related histology, protein expression, and ultrastructure in orthotopic xenografts (27). In contrast, mice with photoreceptor-specific inactivation of *Rb1* or combined inactivation of *Rb1*, *Rbl1*, and *Tp53* failed to produce cone-derived retinoblastomas (28), although *Rb1* loss or combined *Rb1*/*Rbl1*/*Tp53* loss at the retinal progenitor cell stage permitted subsequent cone precursor cell-cycle entry and limited proliferation (11, 29). These findings suggest that *Rb1*-null mouse cone precursors lack features that enable extensive proliferation and tumorigenesis in their human counterparts.

To probe the basis for the human but not mouse cone precursors' proliferative response to RB loss, we aimed to identify the developmental stage at which human RB-deficient cone precursors proliferate, to characterize murine Rb-depleted cone precursor responses at the equivalent stage, and to determine if ectopic expression of oncoproteins (MDM2 and MYCN) that are intrinsically highly expressed in human but not mouse cone precursors enables Rb-depleted mouse cone precursor proliferation. We also examined the longer-term behavior of RB-depleted cone precursors in human retina cultures. Our findings reveal that RB-depleted maturing human but not mouse cone precursors recapitulate important events in human retinoblastoma genesis and suggest that fundamental differences in murine and human cone precursors may challenge the development of ontogenically accurate retinoblastoma models.

Results

RB Depletion Induces Cell-Cycle Entry Solely in Maturing (ARR3$^+$) Human Cone Precursors. As prior studies suggested that retinoblastomas originate from cone precursors (27), we aimed to define the human cone precursor maturation stage that is sensitive to RB loss. Toward this end, human retinae were cultured on a membrane (30) that largely preserves retinal structure and cell–cell interactions (Fig. 1*A*). With this system, all cell types survived for at least 3 wk except for Brn3$^+$ retinal ganglion cells, which died within 7 d in culture (DIC), likely due to optic nerve transection (31). As the retina develops in a central-to-peripheral gradient (32, 33), these cultures allowed us to assess the effects of RB loss at different cone precursor maturation states as revealed by topographic position and expression of cone maturation markers (Fig. 1*A*). As a proxy for the onset of cone maturation, we immunostained for ARR3, whose initial expression coincides with the emergence of cone outer segments and the appearance of apically positioned concentrated actin filaments that are implicated in outer segment development (*SI Appendix*, Fig. S1).

To assess the effects of RB loss, retinae were transduced with lentivirus that coexpressed YFP and either a validated *RB1*-directed shRNA (pLKO.1C-YFP-sh*RB733*) or a nontargeting scrambled shRNA control (pLKO.1C-YFP-sh*SCR*) (Fig. 1*B*) (27). After 12 DIC, retinae were EdU-labeled, sectioned, stained

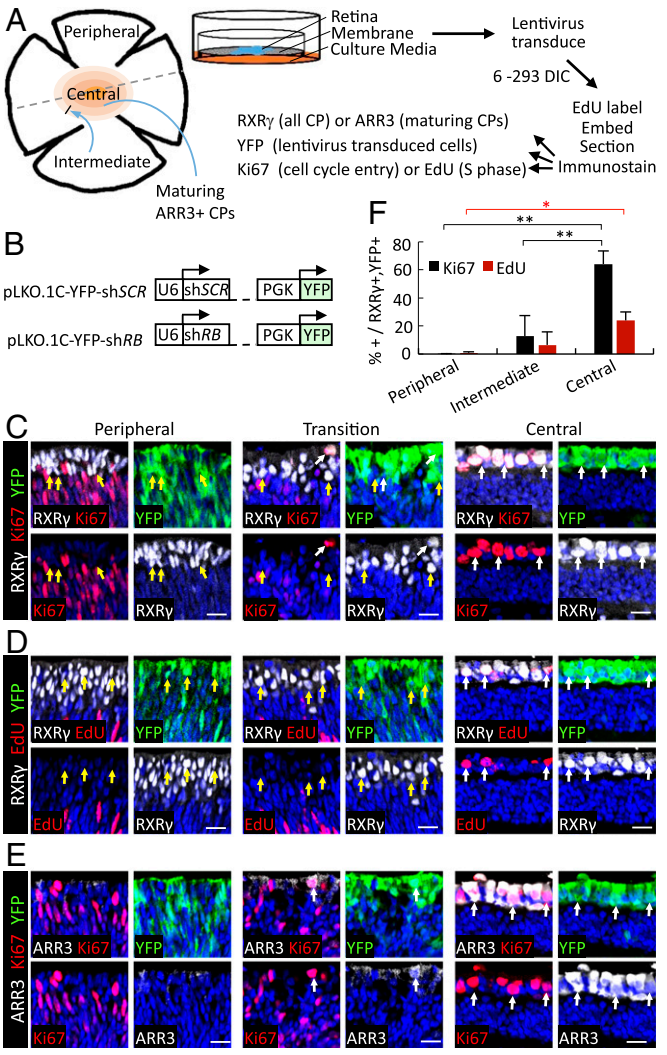

Fig. 1. RB depletion induces cell-cycle entry in maturing (ARR3$^+$) human cone precursors. (*A*) Explanted retinae were cultured on membrane, transduced with shRNAs, and EdU-labeled. Retina shading depicts progressive cone precursor maturation. The dashed line depicts a retina section that may be used to compare cone precursors according to topographic position. (*B*) Lentiviral constructs for retina transduction. (*C*–*E*) Week 18 retinae examined at 12 d after RB KD in peripheral or central retina or in a transition zone with the most peripheral ARR3$^+$ cells. Images show cone markers (RXRγ or ARR3, white), cell-cycle markers (Ki67 or EdU, red), lentivirus-transduced cells (YFP, green), and nuclei (blue). (Scale bars, 20 μm.) (*F*) Percent of Ki67$^+$ or EdU$^+$ cells among RXRγ$^+$,YFP$^+$ cone precursors in each region. Error bars indicate SD. Significance was assessed by *t* test (*$P < 0.01$, **$P < 0.001$).

either for RXRγ to identify all cone precursors (34, 35) or for ARR3 to identify maturing cone precursors, for YFP to identify transduced cells, and either for Ki67 to detect cell-cycle entry or for EdU to monitor S-phase entry (Fig. 1*A*). At 12 DIC, YFP was detected throughout the retina, indicative of transduction of all retinal layers (*SI Appendix*, Fig. S2). However, as YFP was strongest in the cone-rich outer nuclear layer, imaging was optimized to resolve YFP$^+$ cells in these regions.

In retinae explanted and sh*RB1*-transduced at week 18, most YFP$^+$,RXRγ$^+$ cone precursors in the more mature central retina were Ki67$^+$, and many incorporated EdU (Fig. 1 *C*, *D*, and *F*). All Ki67$^+$ and EdU$^+$ cells in this region were strongly ARR3$^+$, indicative of their ongoing maturation (Fig. 1*E*). In contrast, YFP$^+$,RXRγ$^+$ cone precursors in the immature peripheral retina lacked ARR3 and failed to express Ki67 or incorporate EdU

(Fig. 1 *C–F*). At intermediate positions where cone precursors weakly expressed ARR3, a low proportion of YFP$^+$,ARR3^{weak} cells entered the cell cycle, and no YFP$^+$,ARR3$^-$ cells entered the cell cycle (Fig. 1 *C–F*). Retinae transduced with the sh*SCR* control had no Ki67 or EdU incorporation in YFP$^+$,RXRγ$^+$ cone precursors, although both sh*SCR*-transduced and sh*RB1*-transduced retinae had the expected Ki67$^+$,RXRγ$^-$ retinal progenitor cells or glia (27) in the peripheral retina neuroblastic layer (*SI Appendix*, Fig. S3). Thus, in intact human retina, RB-depleted cone precursors acquired the ability to enter the cell cycle at a maturation stage coinciding with the onset of ARR3 expression.

Rb Loss Induces Cell-Cycle Entry in Immature (Arr3$^-$) but Not in Maturing (Arr3$^+$) Murine Cone Precursors. We next asked if Rb loss enables murine cone precursor proliferation at the same developmental stage as in cultured human retina. To examine effects of Rb loss on murine cone precursors in vivo, we produced mice carrying Cre-dependent *Rb1^{lox}* alleles (36) and expressing Cre recombinase under control of the cone-specific red green pigment promoter (*RGP*, also known as "*Opn1lw*") (37). The *RGP* promoter is active in mouse cones beginning at approximately postnatal day (P) 8, soon after Arr3 protein is first detected (38, 39). At both P10 and P28, Rb was readily detected in Rxrγ$^+$ or Arr3$^+$ cone cells in control *Rb1$^{lox/lox}$* mice but not in *RGP-Cre;Rb1$^{lox/lox}$* littermates (Fig. 2*A* and *SI Appendix*, Fig. S4, white arrows). In contrast, Rb was equally prominent in inner nuclear layer cells of both genotypes (Fig. 2*A* and *SI Appendix*, Fig. S4, yellow arrows). Thus, *RGP-Cre;Rb1$^{lox/lox}$* mice were expected to reveal effects of cone precursor-specific Rb loss beginning at or before P10, soon after the onset of Arr3 expression. However, no Ki67 signal was detected among 2,221 Arr3$^+$ or L/M-opsin$^+$ cones examined at P8, P10, P15, and P28 (Fig. 2*B*). Furthermore, none of 50 *RGP-Cre;Rb1$^{lox/lox}$* mice formed retinal tumors at 6–12 mo of age, and no retinomas or other hyperplasias were detected among three histologically examined retinae. Thus, *Rb1* knockout in maturing murine cone precursors failed to induce cell-cycle entry or tumorigenesis.

The lack of cone precursor cell-cycle entry in *RGP-Cre; Rb1$^{lox/lox}$* mice contrasted with the response of maturing (ARR3$^+$) cone precursors in cultured human retinae. To determine whether maturing murine cone precursors can enter the cell cycle when Rb is depleted ex vivo, under the same conditions used to examine human retinae, a validated murine *Rb1*-directed shRNA (40) was delivered into explanted murine retinae using the same YFP-marked lentiviral vector used for human retina analyses. We first examined the effects of Rb knockdown (KD) on murine retinae explanted at P9, similar to the age of *Rb1* knockout in *RGP-Cre; Rb1$^{lox/lox}$* mice. sh*Rb1* transduction was confirmed to deplete Rb protein in cones and other cells (Fig. 2*C*) but did not induce Ki67 or EdU incorporation in Arr3$^+$,YFP$^+$ cells at 7 or 14 DIC (Fig. 2*D*). Thus, Rb depletion failed to induce cell-cycle entry in maturing Arr3$^+$ murine cone precursors under conditions in which ARR3$^+$ human cone precursors robustly entered the cell cycle.

The Rb-deficient Arr3$^+$ murine cone precursors' inability to enter the cell cycle both in vivo (after *RGP-Cre*–mediated disruption at ∼P8) and in vitro (after *shRb1* transduction at P9) contrasted with the prior detection of Ki67$^+$ cone precursors at P8 after *Rb1* knockout in retinal progenitor cells (11). In that study, the Ki67$^+$ cone precursors observed at P8 most likely lacked Rb from the time they were born [between embryonic days (E) 10–16 (41)] and were immature (Arr3$^-$). To determine if Rb depletion of immature murine cone precursors can elicit cell-cycle entry, murine retinae were explanted and transduced at P4, which is ∼6 d after cone genesis is completed (41) and ∼2 d before the onset of Arr3 expression (*SI Appendix*, Fig. S1 and ref. 38). Rb KD in P4 explants induced Ki67 expression and EdU

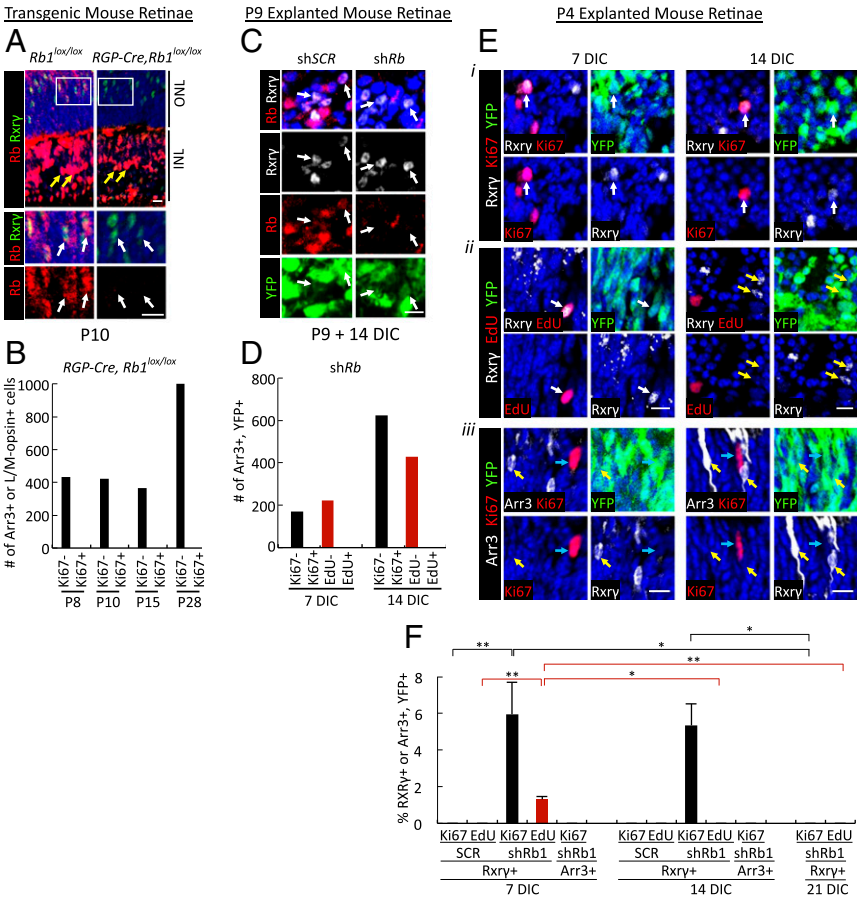

Fig. 2. *Rb1* loss induces cell-cycle entry in immature (Arr3$^-$) murine cone precursors. (*A*) Cone-specific *Rb1* knockout in *RGP-Cre;Rb1$^{lox/lox}$* but not in littermate *Rb1$^{lox/lox}$* mouse retinae at P10. (*Upper*) Sections traversing the outer nuclear layer (ONL) and inner nuclear layer (INL). (*Lower*) Enlarged views of boxed regions. White arrows indicate Rxrγ$^+$ cones; yellow arrows indicate Müller glia. (*B*) The number of Arr3$^+$ or L/M-opsin$^+$ cells analyzed for Ki67 in *RGP-Cre,Rb1$^{lox/lox}$* retinae at various ages. (*C*) P9 explanted retinae transduced with sh*Rb1* or sh*SCR* and stained for Rb, Rxrγ, and YFP at 14 DIC. Arrows indicate Rb staining in sh*SCR*- but not sh*Rb1*-transduced YFP$^+$,Rxrγ$^+$ cone precursors. (*D*) The number of Arr3$^+$,YFP$^+$ cells analyzed for Ki67 and EdU at 7 and 14 DIC. (*E*) P4-explanted and sh*Rb1*-transduced retinae costained for Rxrγ or Arr3 (white), YFP (green), and Ki67 or EdU (red). Examples of outer nuclear layer Rxrγ$^+$,YFP$^+$,Ki67$^+$ (*i*), Rxrγ$^+$,YFP$^+$,EdU$^+$ (*ii*), and Arr3$^+$,YFP$^+$,Ki67$^-$ (*iii*) cells at 7 and 14 DIC are shown. White arrows indicate proliferation marker-positive cone precursors; yellow arrows indicate proliferation marker-negative cone precursors; blue arrows indicate proliferation marker-positive Arr3$^-$ cells. (*F*) Quantitation of YFP$^+$,Rxrγ$^+$ or YFP$^+$,Arr3$^+$ cells from explanted P4 retinae costained for Ki67 or EdU, transduced with sh*Rb1* or sh*SCR*, and analyzed at 7, 14, and 21 DIC. Error bars indicate SD. Significance was assessed by ANOVA with Tukey's HSD post hoc test (*$P < 0.05$, **$P < 0.001$). (Scale bars, 10 μm.)

incorporation in Rxrγ$^+$ cones at 7 DIC, in Ki67$^+$ but not EdU$^+$ cones at 14 DIC, and in neither Ki67$^+$ nor EdU$^+$ cones at 21 DIC (Fig. 2 *E* and *F*). As we did not detect cleaved caspase 3$^+$,Rxrγ$^+$ cells, the Rb-depleted cone precursors most likely had not died but had exited the cell cycle, consistent with the presence of surviving *Rb1*$^{-/-}$ cone precursors in vivo (11). Notably, in P4 explanted retina, Arr3 was induced in a subset of cone precursors after 7 and 14 DIC, indicative of maturation in vitro. However, whereas ∼5% of Rxrγ$^+$ cone precursors were Ki67$^+$, no Arr3$^+$ cone precursors were Ki67$^+$ at 7 or 14 DIC (Fig. 2 *E*, *iii* and *F*). Thus, Rb KD at P4 enabled limited cell-cycle entry of postmitotic immature (Arr3$^-$) but not maturing (Arr3$^+$) murine cone precursors.

MDM2 and Mycn Promote Cell-Cycle Entry of Immature but Not Maturing Murine Cone Precursors. The cell-cycle entry of RB-depleted maturing (ARR3$^+$) human but not murine cone precursors suggested that maturing murine cone precursors lack proliferation-related circuitry that is present in their human counterparts. As ARR3$^+$ human but not mouse cone precursors prominently express MDM2 and MYCN (24), and as MDM2 and MYCN were critical to the RB-depleted human cone precursors' proliferation (27), we examined whether increased MDM2 and/or Mycn can enable Rb-deficient maturing murine cone precursor proliferation in our in vivo and in vitro models.

Since MDM2 promotes MYCN expression in retinoblastoma cell lines (42), we first explored whether ectopic MDM2 induces endogenous Mycn expression and Rb-deficient cone precursor proliferation in the *RGP-Cre;Rb1*$^{lox/lox}$ background. As MDM2 is initially expressed at the onset of ARR3 expression in the human retina (*SI Appendix*, Fig. S5), we simulated the timing of human cone precursor MDM2 expression using an *RGP-MDM2* transgene (Fig. 3*A*), which is induced at or soon after the onset of Arr3 expression (38, 39). The transgene expressed the full-length human MDM2-X1 isoform produced from the p53-regulated *MDM2 P2* promoter (43), chosen because the cone-related RXRγ up-regulates the *P2* promoter (24). In each of five transgenic strains, MDM2 was first detected in L/M-opsin$^+$ or Arr3$^+$ cones at P9, and expression increased at P15 and P20 (Fig. 3 *B* and *C*), resembling the timing of human MDM2 expression (*SI Appendix*, Fig. S5). However, *RGP-MDM2;RGP-Cre;Rb1*$^{lox/lox}$ retinae showed no higher Mycn than wild-type controls at P10 and P20 (*SI Appendix*, Fig. S6*A*), no Ki67$^+$ cells among 1,499 Arr3$^+$ or L/M-opsin$^+$ cells examined at P8–P20 (Fig. 3*D*), and no tumors among 62 6- to 12-mo-old mice. Thus, ectopic MDM2 did not enable maturing *Rb1*-null mouse cone precursors to induce Mycn or enter the cell cycle in vivo.

We next examined the effects of ectopic MDM2 and Mycn on Rb-deficient murine cone precursors under the in vitro culture conditions that enabled human cone precursor proliferation (Fig. 4*A*). In these studies, MDM2 was expressed from the *RGP-MDM2* transgene with timing similar to that in vivo; Rb depletion was confirmed; and either wild-type Mycn or a stabilized Mycn protein (Mycn^{T58A}) (44) was expressed from the BE-Neo (BN) lentiviral vector (*SI Appendix*, Fig. S6 *B–D*). Transduction of P9 retinae with BN-Mycn enabled two- to sixfold overexpression in ∼10% of Rxrγ$^+$ cone precursors, whereas transduction of P4 retinae with BN-Mycn^{T58A} enabled two- to sixfold Mycn overexpression in ∼13% of infected Rxrγ$^+$ cone precursors (*SI Appendix*, Fig. S6 *E* and *F*).

In the in vitro setting, transduction of explanted P9 *RGP-MDM2* retinae with sh*Rb1* and ectopic Mycn failed to induce Ki67 at 7 or 14 DIC either when transduced individually or after cotransduction (Fig. 4*B*). Thus, ectopic MDM2 and Mycn failed to promote cell-cycle entry in Rb-depleted maturing (Arr3$^+$) murine cone precursors.

In contrast, ectopic MDM2 and Mycn promoted cell-cycle entry in immature (Arr3$^-$) murine cone precursors after transduction of P4 retinae. Specifically, transgenic MDM2 prolonged the Rb-depleted immature cone precursors' capacity for S-phase entry, as Rb KD induced similar proportions of EdU positivity in

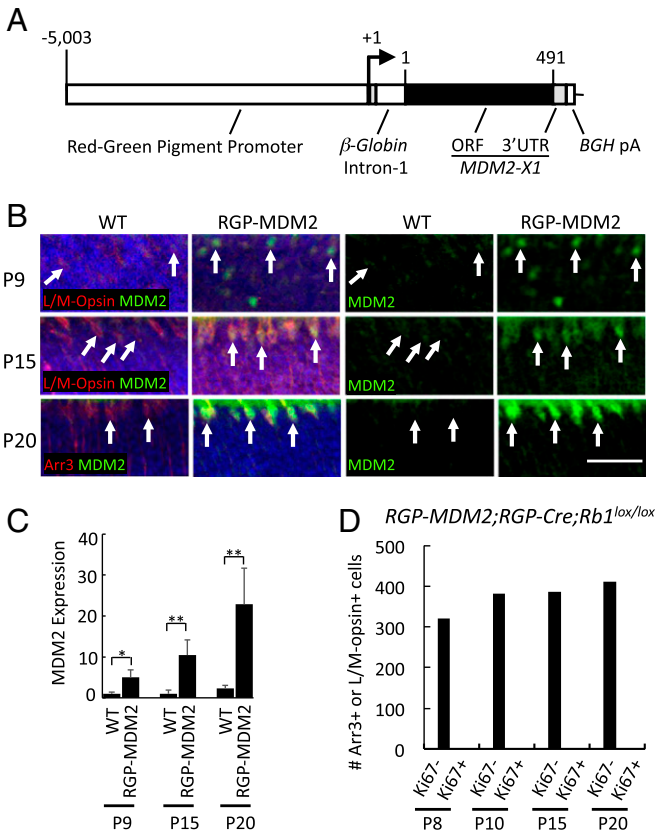

Fig. 3. Cone precursor-specific MDM2 expression fails to sensitize murine cone precursors to *Rb1* knockout in vivo. (*A*) *RGP-MDM2* transgene with the *RGP* (*Opn1lw*) promoter, *β-globin* intron, human *MDM2* isoform X1 ORF, and bovine growth hormone poly(A) (BGH pA). Numbers indicate the *RGP* promoter base pair position relative to the transcription start site and MDM2-X1 amino acid positions. (*B*) Expression of human MDM2 (green) in L/M-opsin$^+$ or Arr3$^+$ (red) cones in *RGP-MDM2* transgenic but not in wild-type mice at P9, P15, and P20. (*C*) Quantitation of MDM2 expression in L/M-opsin$^+$ or Arr3$^+$ cells in *RGP-MDM2* versus WT mice. Error bars indicate SD. (*D*) The number of Arr3$^+$ or L/M-opsin$^+$ cells analyzed for Ki67 expression at various ages in *RGP-MDM2;RGP-Cre;Rb1*$^{lox/lox}$ retinae. (Scale bar, 20 μm.) Significance was assessed by *t* test (*$P < 0.05$, **$P < 0.001$).

cone precursors in wild-type and *RGP-MDM2* retinae at 7 DIC and induced EdU incorporation in *RGP-MDM2* but not wild-type retinae at 14 DIC (Fig. 4 *C* and *D*). Furthermore, transduction of Mycn^{T58A} on its own induced low-level Ki67 expression at 7 DIC and both Ki67 and EdU incorporation at 14 DIC (Fig. 4 *C* and *D*). However, cotransduction with *Mycn*^{T58A} and sh*Rb1* failed to increase Ki67 expression or EdU incorporation over that induced by sh*Rb1* alone in either wild-type or *RGP-MDM2* retinae (Fig. 4 *C* and *D*). Similarly, cotransduction of *RGP-MDM2* retinae with *Mycn*^{T58A} and sh*Rb1* failed to sustain Ki67 expression through 21 DIC or to induce Ki67 expression in Arr3$^+$ cells (Fig. 4*E*). Thus, in explanted P4 retinae, Mycn^{T58A} induced proliferation in a small proportion of immature cone precursors but did not augment proliferative responses to Rb loss and failed to enable proliferation of maturing (Arr3$^+$) cone precursors.

RB-Depleted Human but Not Mouse Cone Precursors Proliferate and Form Retinoma-Like and Retinoblastoma-Like Lesions. The above studies indicated that RB-deficient murine and human cone precursors enter the cell cycle at different developmental stages. However, the murine cell-cycle entry was limited to <21 d, whereas RB-depleted human cone precursors were reported to remain in the cell cycle for at least 23 d and to form retinoblastoma-like tumors in xenografts (27). To investigate this discrepancy, we asked

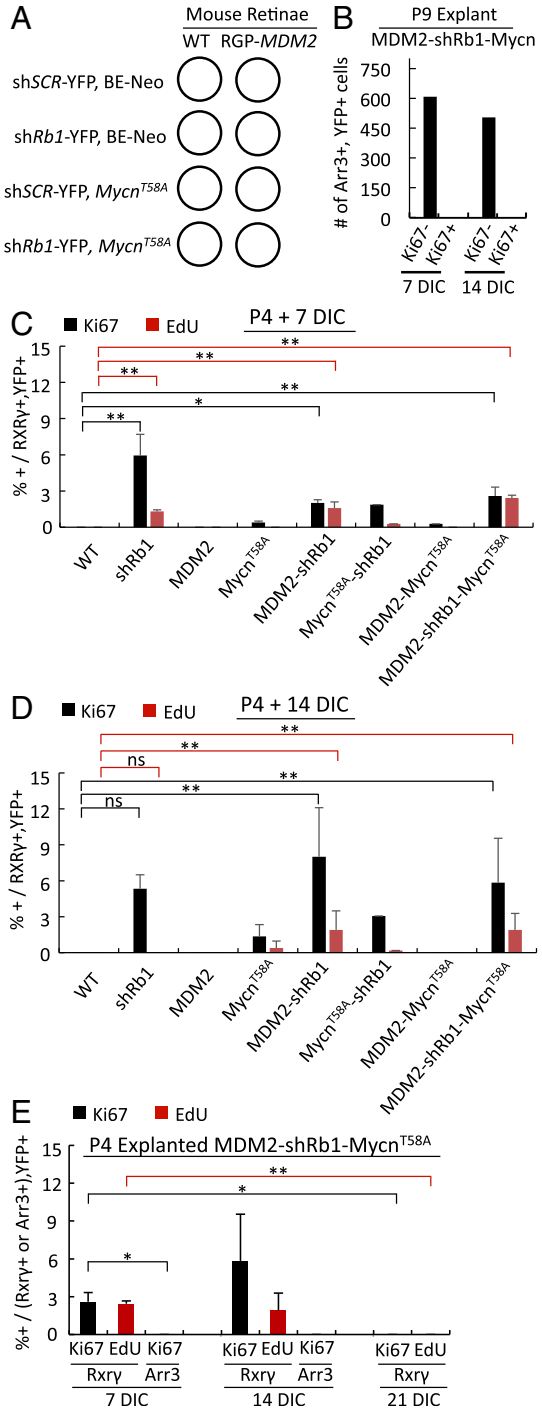

Fig. 4. MDM2 and Mycn promote cell-cycle entry of immature but not maturing murine cone precursors. (*A*) Scheme for lentiviral transduction of WT or *RGP-MDM2* retinae with sh*Rb1* or sh*SCR* and with BE-Neo-*Mycn*^{T58A} or BE-Neo vector. (*B*) The number of YFP$^+$,Arr3$^+$ cells from P9 *RGP-MDM2* explanted and sh*Rb1*- and *Mycn*-transduced retinae analyzed for Ki67 at 7 and 14 DIC. (*C* and *D*) Quantitation of YFP$^+$,Rxrγ$^+$ cells costained for Ki67 or EdU in P4 WT or *RGP-MDM2* retinae at 7 (*C*) or 14 (*D*) DIC. Labels indicate oncogenic variables (sh*Rb1*, MDM2, Mycn) and omit the applied control vectors or WT genotype. (*E*) Quantitation of YFP$^+$,Rxrγ$^+$ cells or YFP$^+$,Arr3$^+$ cells costained for Ki67 or EdU in P4 *RGP-MDM2* retinae transduced with sh*Rb1* and *Mycn*^{T58A} and analyzed at 7, 14, and 21 DIC. Error bars indicate SD. Significance was assessed by ANOVA with Tukey's HSD post hoc test (*$P < 0.05$; **$P < 0.001$, ns, not significant).

if RB-depleted murine and human cone precursors in explanted retinae merely enter or also complete the cell cycle. We focused on the expression of cyclin B1, which normally accumulates in G2 and M, and on the mitosis-associated phospho-histone H3-Ser10 (pH3-S10). In sh*RB1*-transduced human retinae examined at 12 DIC, RXRγ$^+$ cone precursors expressed cyclin B1 and pH3-S10 in a central-to-peripheral gradient (Fig. 5 *A* and *C*) similar to that of Ki67 and EdU (Fig. 1*F*). In contrast, sh*Rb1*- and Mycn^{T58A}-transduced *RGP-MDM2* mouse cone precursors induced neither cyclin B1 nor pH3-S10 (Fig. 5 *B* and *D*), implying that Rb-depleted and MDM2- and Mycn-overexpressing immature murine cone precursors can enter but fail to complete the cell cycle.

We next explored the subsequent fate of the RB-depleted human cone precursors. At 30 and 74 DIC, many sh*RB1*-transduced cone precursors, identified by YFP and RXRγ coexpression, were Ki67$^+$ and EdU$^+$ (Fig. 6 *A*–*D*), although the EdU$^+$ proportion declined relative to that observed at 12 DIC (Fig. 6*E*). The cultured retinae also took on a hyperplastic and disorganized appearance with abundant Flexner–Wintersteiner rosettes resembling a retinoblastoma tumor (Fig. 6 *F*–*H*). The Flexner–Wintersteiner rosettes' ring-like distribution of nuclei was also evident in immunostaining (Fig. 6 *A*–*D*, yellow circles), which revealed that the rosettes were largely comprised of RXRγ$^+$ cells, many of which were Ki67$^+$ or EdU$^+$. Flexner–Wintersteiner rosettes were not evident in human retinae transduced with control sh*SCR* and cultured in parallel (Fig. 6*I*) or in Rb-depleted murine retinae either with or without ectopic MDM2 and Mycn (*SI Appendix*, Fig. S7). Some retinal regions

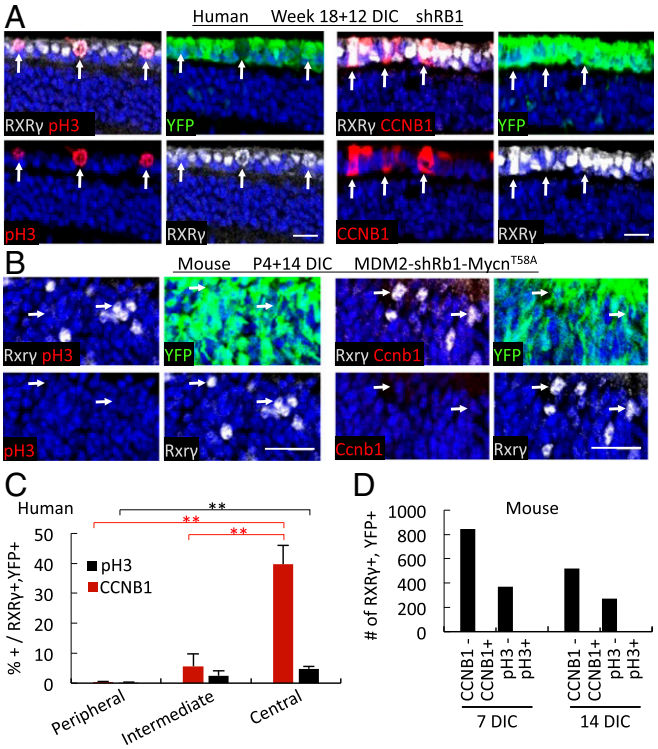

Fig. 5. Rb-depleted human but not mouse cone precursors express G2 and M-phase markers. (*A* and *B*) Cyclin B1 (CCNB1) and phospho-histone H3-Ser10 (pH3) (red) in RXRγ$^+$ (white) cone precursors of 18 wk human retinae at 12 d after RB KD (*A*) but not in Rxrγ$^+$ (white) cone precursors of P4 *RGP-MDM2* mouse retinae at 14 d after Rb KD and Mycn overexpression (*B*). (Scale bars, 20 μm.) (*C*) The percentage of CCNB1$^+$ or pH3$^+$ cells among RXRγ$^+$,YFP$^+$ cone precursors in human retina sections adjacent to those stained for Ki67 and EdU in Fig. 1*F*. (*D*) The number of RXRγ$^+$,YFP$^+$ cells analyzed for CCNB1 or pH3 in *RGP-MDM2* retinae cotransduced with sh*Rb1* and *Mycn*^{T58A} at 7 and 14 DIC. Error bars indicate SD. Significance was assessed by *t* test (**$P < 0.001$).

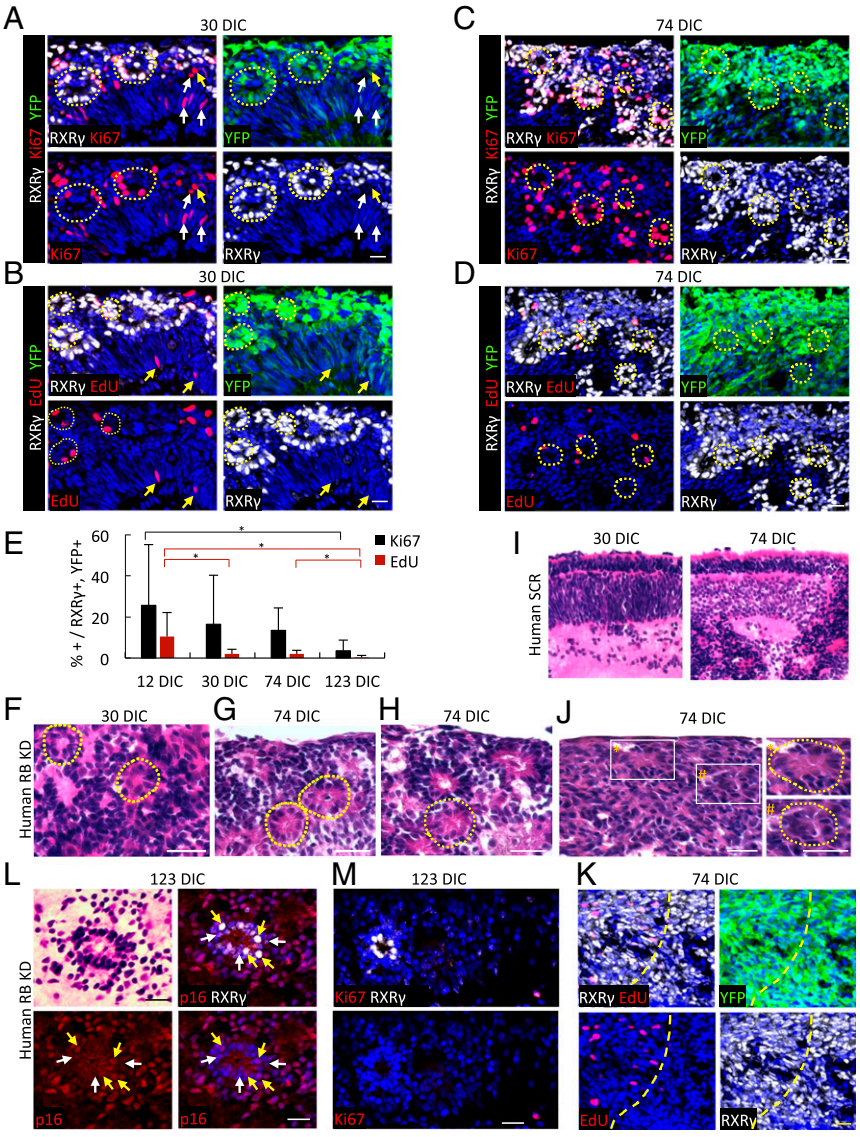

Fig. 6. Cone precursor proliferation and retinoma genesis in RB-depleted human but not mouse retinae. (*A–D*) Ki67 expression (*A* and *C*) and EdU incorporation (*B* and *D*) (red) at 30 DIC (*A* and *B*) and 74 DIC (*C* and *D*) after transduction of week 18 fetal retinae. Dashed circles identify rosette-like arrangements of RXRγ$^+$ nuclei. Arrows indicate proliferating transduced (yellow arrows) or nontransduced (white arrows) noncone (RXRγ$^-$) cells likely representing progenitors or glia. (*E*) Quantitation of Ki67 expression and EdU incorporation in RXRγ$^+$ cone precursors in week 18 retinae at 12–123 DIC. Data at each age are from central, intermediate, and peripheral regions. Error bars indicate SD. Significance was assessed by ANOVA with Tukey's HSD post hoc test (*$P < 0.05$). (*F–J*) H&E staining of week 18 retinae at the indicated DIC after transduction with sh*RB1* (*F–H* and *J*) or sh*SCR* (*I*). Dashed circles identify Flexner–Wintersteiner rosettes (*F–H*) or fleurettes (*J*, *Right*). (*Left*) Enlarged views of boxed regions. (*K*) Predominance of RXRγ$^+$,YFP$^+$ cells in the retinoma-like region shown in *J*. The dashed yellow line separates proliferating (upper left) and nonproliferating (lower right) regions. (*L*) H&E staining (*Upper Left*) performed after p16^{INK4A} immunostaining and imaging of RB-depleted retina at 123 DIC, showing a central fleurette with predominantly cytoplasmic p16 in RXRγ^{lo} cells (white arrows) and nuclear p16 in RXRγ^{hi} cells (yellow arrows). (*M*) A fleurette composed of RXRγ$^+$,Ki67$^-$ cells at 123 DIC. (Scale bars, 20 μm.)

also had Ki67$^+$,RXRγ$^-$ cells (i.e., proliferating noncone cells); however, some of these were YFP$^-$, indicating that they were not sh*RB1*-transduced (Fig. 6 *A* and *B*, white arrows), and similar Ki67$^+$ cells were present in retinae transduced in parallel with the sh*SCR* control (*SI Appendix*, Fig. S3), suggesting that they represent proliferating retinal progenitor cells or glia. Thus, in cultured retinae, RB depletion enabled cone precursor cell-cycle entry within 12 DIC and enabled proliferation and development of retinoblastoma-like lesions at 30 and 74 DIC.

At 123 DIC, RXRγ$^+$,YFP$^+$ cells continued to be detected, but Ki67$^+$ and EdU$^+$ cells were significantly rarer (Fig. 6*E*). Although the sections analyzed at different DIC were from different retinal regions, the temporal decline in proliferation markers was evident by 74 DIC in regions of disorganized RXRγ$^+$ cells (Fig. 6 *J* and *K*). Similar features were seen at 119 DIC in an independently transduced retina. Thus, most but not all of the previously highly proliferating RB-depleted cone precursors appear to exit the cell cycle over ∼4 mo, suggesting that the lesions enter a slowly changing indolent phase.

As the increase in nonproliferating RB-depleted cone precursors was consistent with the production of premalignant retinomas (2), we explored whether cultured retina cone precursor lesions had retinoma-associated features including fleurettes (19) and p16 and p130 expression (2). Indeed, retinae transduced with *RB1*-directed shRNA formed fleurettes within highly RXRγ$^+$ regions at 74 DIC (Fig. 6 *J* and *K*) and formed numerous fleurettes that lacked Ki67 but expressed p16 at 123 DIC (Fig. 6 *L* and *M*). Quantitative immunofluorescence imaging revealed that the sh*RB1*-transduced (YFP$^+$) cone precursors at 12, 30, and 74 DIC had increased p16 and p130 relative to retinae from the fellow eye transduced with sh*SCR* shRNA control (Fig. 7 *A* and *B* and *SI Appendix*, Fig. S7 *A* and *B*). Notably, p16 was mainly nuclear in the RXRγ^{hi} cells that predominated at 12 and 30 DIC and was present at 123 DIC (Fig. 6*L* and *SI Appendix*, Fig. S8*A*) but was mainly cytoplasmic in the RXRγ^{lo} cells that were more common at 123 DIC (Fig. 6*L*), as reported for patient-derived retinoma samples (2). In contrast, Rb-depleted murine retinae with ectopic MDM2 and Mycn lacked increased cone precursor p16 or p130 (Fig. 7 *C* and *D* and *SI Appendix*, Fig. S8 *C* and *D*). Thus, maturing human but not murine cone precursors proliferated and formed retinoma-like lesions in response to RB loss.

The above analyses revealed features of retinoblastoma starting at 30 d after RB KD and features of retinoma at 74, 119, and 123 d after RB KD. To assess whether RB KD can result in full-blown retinoblastoma, we cultured RB-depleted week 19 and week 21 retinae for longer times. In both retinae, cell masses became visible starting at ∼8 mo after RB KD and were detected in all quadrants by 9 mo after RB KD (Fig. 8*A*). Histologic examination revealed

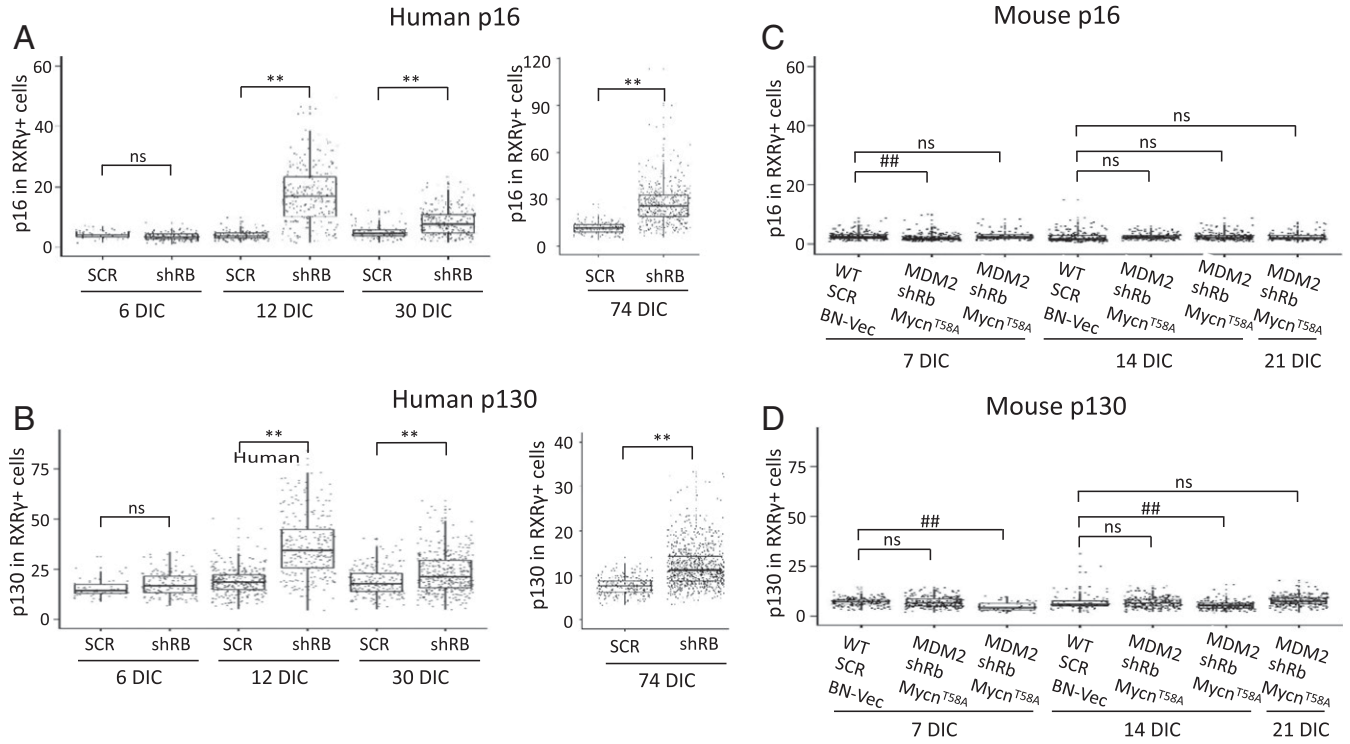

Fig. 7. Cone precursor expression of the retinoma-related p16^{INK4A} and p130 in RB-depleted human but not mouse retinae. Quantitation of p16 and p130 protein in RXRγ^{+},YFP^{+} cells in human retinae at 6, 12, 30, and 74 d posttransduction with sh*RB1* or sh*SCR* (*A* and *B*) and in P4 WT or *RGP-MDM2* mouse retinae at 7, 14, and 21 d posttransduction with sh*SCR*, sh*Rb1*, BN vector, or BN-*Mycn*^{T58A} (*C* and *D*), based on immunostaining shown in *SI Appendix*, Fig. S8. Each dot represents a quantitatively imaged RXRγ^{+},YFP^{+} cell outlined by RXRγ signal. Box plots show median, upper and lower quartiles (box borders), and data range (whiskers). Significance was assessed by *t* test (**$P < 0.0001$; $^{\#\#}P < 0.0001$; ns, not significant).

numerous Flexner–Wintersteiner rosettes (Fig. 8*B*), consistent with a differentiated retinoblastoma phenotype. The mass was mainly composed of RXRγ^{+} cells that were in the cell cycle as determined by Ki67 expression (Fig. 8*C*). Interestingly, cytoplasmic p16 was evident in proliferating RXRγ^{hi} cells that retained a differentiated histology (Fig. 8*D*) which differed from the nuclear p16 in RXRγ^{hi} cells at earlier time points (Fig. 6*L* and *SI Appendix*, Fig. S8*A*).

Discussion

This study examined the effects of RB loss on developing cone precursors in intact human and mouse retinae. We report that RB-depleted human maturing (ARR3^{+}) cone precursors enter the cell cycle, proliferate, and form retinoma- and retinoblastoma-like lesions, whereas Rb-depleted murine immature (Arr3^{-}) cone precursors enter but do not complete the cell cycle (Fig. 9). Maturing Arr3^{+} murine cone precursors failed to enter the cell cycle both in response to *Rb1* knockout in vivo and in response to Rb knockdown initiated either before or after the onset of Arr3^{+} expression (Fig. 2). Moreover, ectopic MDM2 and Mycn did not enable maturing murine cone precursor cell-cycle entry either in vivo or under in vitro conditions identical to those that enabled human cone precursor proliferation (Figs. 3 and 4). These findings are consistent with past evidence that murine cone precursors fail to proliferate after photoreceptor-specific *Rb1* knockout or combined *Rb1*, *Rbl1*, and *Tp53* knockout (28). Thus, maturing (Arr3^{+}) murine cone precursors show an impressive resistance to cell-cycle entry, whereas maturing (ARR3^{+}) human cone precursors show an impressive propensity to proliferate under the same conditions.

Our findings imply that RB is not needed to enforce cell-cycle exit at the time of human cone precursor cell birth but acquires this role coincident with the onset of ARR3 expression and outer segment growth (Fig. 1 and *SI Appendix*, Fig. S1). As outer segment morphogenesis was proposed to reflect the start of a distinct second phase of vertebrate photoreceptor differentiation (45), our data suggest that human cone precursors become sensitized to RB loss during this second phase. Concordantly, RB is barely detectable in immature cone precursors (34, 46) and increases to far higher levels during human versus mouse cone maturation (24, 34). Thus, RB's role in suppressing human cone precursor cell-cycle entry correlates with its increased expression during human cone precursor maturation. If sensitivity to RB loss also correlates with maturation (i.e., ARR3 expression) in vivo, then the first aberrant proliferation of RB-deficient cone precursors may occur at the onset of ARR3 expression, at approximately week 15 in the central retina (47), ∼6 wk after the first cone precursors are born at approximately week 8 or 9 (48). A similar interval between cone cell birth and sensitivity to RB loss may apply as cone genesis propagates to the far periphery by week 22 (49).

Our finding that RB-depleted maturing (ARR3^{+}) but not immature (ARR3^{-}) human cone precursors enter the cell cycle suggests that human cone maturation is associated with increased mitogenic signaling. Indeed, cone precursor maturation is associated with increased MDM2 and MYCN in humans but not in mice (Fig. 3, *SI Appendix*, Fig. S5, and ref. 24). Although MDM2 and MYCN were needed for the human cone precursor proliferative response to RB loss (27), ectopic MDM2 and Mycn did not enable cell-cycle entry in Rb-deficient maturing murine cone precursors (Fig. 4). As a caveat, the ectopic Mycn might not have been overexpressed to a sufficient level to enable maturing cone precursor proliferation in these experiments. However, maturing mouse cone precursors were resistant to ectopic Mycn overexpression compared with maturing human cone precursors transduced with the same methods, suggesting that additional, potentially mitogenic, signals enable high-level MYCN expression during human but not murine cone maturation. Indeed, maturing human cone precursors express a larger proliferation-related program, beyond high-level MDM2 and MYCN (50), that could contribute to the proliferative response to RB loss.

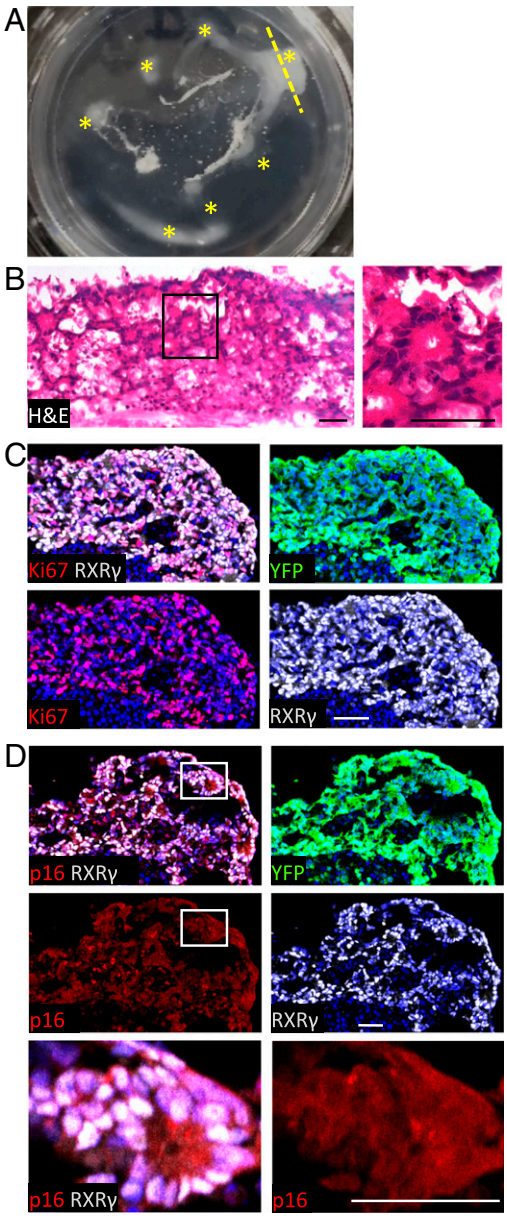

Fig. 8. RB-depleted retinal explants form retinoblastoma-like masses. (*A*) Explanted retina cultured for 293 d after RB KD. At least seven distinct cell masses were observed (asterisks). The yellow dashed line indicates the plane of the section used for H&E and immunostaining. (*B*) H&E staining reveals retinoblastoma-like histology including Flexner–Wintersteiner rosettes. The boxed region is enlarged at the right. (*C* and *D*) Ki67 (*C*) and low-level cytoplasmic $p16^{INK4A}$ (*D*) are detected throughout the mass. The boxed region in *D* is enlarged in the bottom row. (Scale bars, 40 μm.)

While maturing murine cone precursors did not acquire proliferative potential, prior studies suggested that another murine postmitotic cell type—horizontal cells—can proliferate and form tumors in response to combined biallelic loss of *Rb1*, biallelic loss of *Rbl2* (encoding p130), and monoallelic loss of *Rbl1* (encoding p107) (25). Like maturing human cone precursors, murine $Prox1^{+}$ horizontal and amacrine cells have intrinsically high Mdm2 (24), possibly reflecting a similar tumor-prone state. Thus, the $Rb1^{-/-}$;$Rbl2^{-/-}$;$Rbl1^{+/-}$ model, as well as other models in which tumors derive from $Prox1^{+}$ interneurons, might simulate an oncogenic process that is analogous but not orthologous to human retinoblastoma genesis.

In contrast to the proliferative response of RB-depleted maturing human cone precursors, only Rb-depleted immature ($Arr3^{-}$) murine cone precursors entered the cell cycle (Fig. 2). Immature murine cone precursor cell-cycle entry was prolonged by ectopic MDM2 and was independently induced by Mycn (Fig. 4), but these responses were far weaker than the ∼60% of maturing human cone precursors that entered the cell cycle in the central retina (Fig. 1*F*). Also, the Rb-depleted and MDM2- and Mycn-overexpressing immature murine cone precursors could enter but could not complete the cell cycle (Fig. 5), reminiscent of Rb-deficient murine hepatocytes (51). Similar to Rb-depleted immature mouse cone precursors in vitro, $Rb1^{-/-}$ immature cone precursors that derived from *Rb1*-knockout retinal progenitor cells entered the cell in vivo (11). Moreover, combined *Rb1* and *Rbl1* knockout enabled immature cone precursor division followed by p53-mediated apoptosis, and further p53 loss enabled their cell-cycle exit and maturation (29). Thus, whereas RB-deficient human cone precursors acquire the ability to proliferate during maturation, aberrantly proliferating *Rb1*/*Rbl1*/*Tp53*-deficient immature cone precursors appear to lose the ability to proliferate during the maturation process.

After entering the cell cycle, RB-depleted human cone precursors formed hyperplasias with Flexner–Wintersteiner rosettes and fleurettes, histologic features specific to retinoblastoma and retinoma, respectively (Fig. 6) (2, 19). Flexner–Wintersteiner rosettes were abundant at 30 d after RB KD, and cells within the rosettes expressed cone markers at levels similar to the earliest proliferating cone precursors, implying that they are the cone precursors' direct descendants (Fig. 9). Retinoma-like lesions detected at 74, 119, and 123 DIC also expressed cone markers (Fig. 6), suggesting that they derive from tissue containing Flexner–Wintersteiner rosettes. These lesions also had largely cytoplasmic p16, particularly in $RXR\gamma^{lo}$ cells, as in patient-derived retinomas (2). After ∼8 mo, RB-depleted retinae formed multiple masses with abundant Flexner–Wintersteiner rosettes, resembling differentiated retinoblastoma tissue (Fig. 8). The proliferating lesions' predominantly cytoplasmic p16 in $RXR\gamma^{hi}$ as well as in $RXR\gamma^{lo}$ cells was a distinct feature not seen in retinoma-like tissue. Further analyses are needed to assess whether cytoplasmic p16 localization enables the transition from indolent proliferation to differentiated retinoblastoma and whether further p16 loss enables a subsequent transition to the dedifferentiated retinoblastomas that were reported to have reduced p16 expression (2).

In conclusion, our data indicate that cell-signaling circuitry that is uniquely associated with human cone precursor maturation sensitizes to the oncogenic effects of RB loss. Our findings suggest that because of this circuitry RB-deficient maturing cone precursors initially form proliferative lesions that resemble differentiated retinoblastomas, in which the majority of cells exit the cell cycle to form nonproliferating retinomas and a minority remain in the cell cycle, possibly in an indolent state, to form retinoblastoma tumors (Fig. 9). Understanding the parameters that enable proliferating RB-deficient cone precursors to enter or bypass the retinoma state could provide opportunities to suppress retinoblastoma in genetically predisposed children.

Materials and Methods

Retinal Tissue. Following informed consent, fetal eyes were obtained from authorized sources with approval by the University of Southern California (USC) and Children's Hospital Los Angeles Institutional Review Board. Gestational age was estimated according American College of Obstetrics and Gynecology guidelines (52). All mouse experiments were approved and performed according to the guidelines of the Institutional Animal Care and Usage Committees of Memorial Sloan-Kettering Cancer Center and The Saban Research Institute of Children's Hospital Los Angeles.

Retinal Culture. Eyes were held on ice for up to 4 h, sterilized in 70% ethanol for 5 s, and submerged in cold PBS. Retinae were harvested, cut radially to flatten, and placed on hydrophilic polytetrafluoroethylene cell-culture inserts (PICM01250 or PICM0RG50; Millipore) with the photoreceptor side down (30). Inserts with retinae were quickly moved to six- or 12-well plates for human and murine cultures, respectively, with 1,200 μL or 250 μL of retina culture medium [Iscove's Modified Dulbecco's Medium (IMDM; Corning), 10% FBS (Sigma-Aldrich), 0.28 U/mL insulin (Lilly), 55 μM β-mercaptoethanol (Sigma-Aldrich),

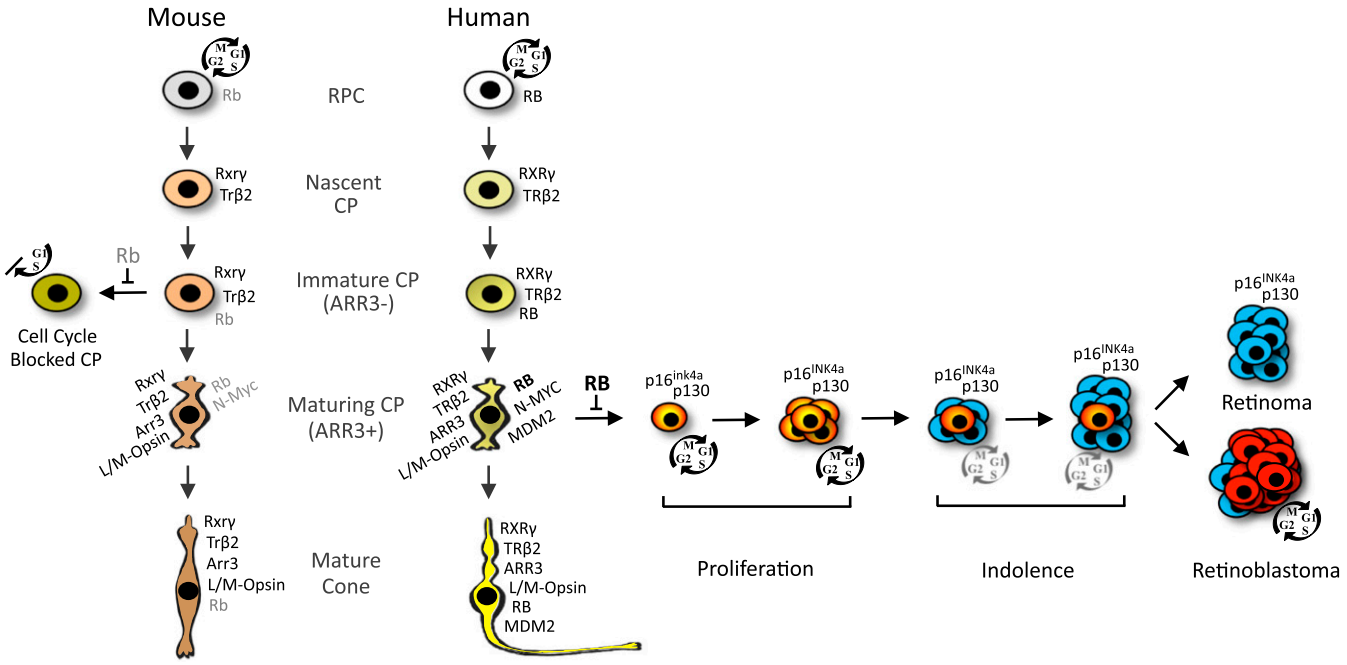

Fig. 9. Distinct responses to RB loss in human and murine cone precursors. The cartoon depicts the generation of cone precursors (CPs) from retinal progenitor cells (RPCs) and the distinct human and mouse CP protein expression and responses to RB loss at different developmental stages. Nascent CPs are RXRγ^{+},TRβ2^{+} and have minimal RB expression in humans (34) and mice (46). RB increases during CP maturation in both species but to far higher levels and in association with N-MYC and MDM2 expression in humans (24, 34, 46). This study shows that in human retinae, RB loss causes maturing (ARR3^{+}) CP cell-cycle entry and proliferation (orange) followed by cell-cycle withdrawal (blue) and an indolent phase that may give rise to permanently quiescent retinomas or to retinoblastoma tumors (red), whereas in mouse retinae, Rb loss causes immature (Arr3^{-}) CP cell-cycle entry but not proliferation or retinoma- or retinoblastoma-like lesions.

glutamine (Sigma-Aldrich), penicillin, and streptomycin (Corning)]. Unused wells and spaces were filled with PBS, and plates were incubated at 37 °C with 5% CO_2. At various time points human retinae were cut into pie-shaped sectors containing central and peripheral regions for embedding and analyses.

Lentiviral Transduction. Frozen concentrated virus was thawed on ice and supplemented with FBS, β-mercaptoethanol, insulin, glutamine, penicillin, and streptomycin to the final concentrations in the retina culture medium along with Polybrene (4 μg/mL; Sigma-Aldrich). Cell-culture inserts were moved to empty wells, and virus was added on top of the retinae. Virus-containing medium flowing through the membrane was replaced on the retina every 15–20 min. After 3 h, cell-culture inserts were returned to wells with fresh medium. Half of the medium was changed every 2 d. Retinae were incubated with EdU (10 U/mL; Invitrogen) for 4 h before harvest and were fixed in fresh 4% paraformaldehyde in PBS for 15 min. After three PBS washes, retinae were equilibrated in sucrose (30% in PBS) for 15 min and embedded in sucrose–O.C.T. mix (2:1; Tissue-Tek) on dry ice, and the blocks were stored at −80 °C. Blocks were sectioned at 10 μm on positively charged slides, and slides were stored at −80 °C.

Lentivirus Production. Lentivirus was produced in 15-cm dishes by reverse transfection of 3×10^7 293T cells using 20 μg lentiviral vector, 5 μg pVSV-G, 10 μg pMDL, and 5 μg pREV in 3 mL of serum-free DMEM-HG (Corning). One hundred twenty microliters of polyethylenimine (PEI) (0.6 μg/mL; Polysciences Inc.) was mixed with 3 mL of serum-free IMDM and was incubated for 20 min at room temperature. Cells were mixed with the PEI mixture and were plated in DMEM-HG medium (Corning) with 10% FBS. At 14–16 h, medium was replaced with serum-free UltraCULTURE medium (Lonza Inc.), and virus was harvested at 60 h posttransfection. The supernatant was centrifuged at 3,000 × *g* for 10 min at 4 °C and filtered with a 0.45-μm polyethersulfone membrane (VWR). Virus was concentrated using tangential flow filtration (53), refiltered using a 0.45-μm PVDF filter (Millipore), stored in aliquots at −80 °C, and titered using a p24 ELISA kit (ZeptoMetrix Corporation).

Mice. *RGP-Cre* (37) and *Rb1$^{lox/lox}$* mice (36) were provided by Anand Swaroop, National Eye Institute, NIH, Bethesda, and David MacPherson, Fred Hutchinson Cancer Research Center, Seattle, respectively. *RGP-Cre* and *Rb1$^{lox/lox}$* mice were obtained in mixed 129/SV and C57BL/6 backgrounds and were backcrossed to C57BL/6J mice (Jackson Laboratories) for at least four generations before breeding with other strains.

RGP-MDM2 mice were produced as follows. The *RGP-MDM2* transgene was produced by cloning the human *MDM2* ORF of RefSeq variant XM_005268872.4, which encodes the 491-aa MDM2 isoform X1, and the flanking vector bovine growth hormone poly(A) site from pcDNA3-MDM2 (kindly provided by Ze'ev Ronai, Sanford Burnham Prebys Medical Discovery Institute, La Jolla, CA) into the BamH1 and PshAI sites 3′ of the rabbit *β-globin* splice acceptor region of p*RGP–β-globin*. p*RGP–β-globin* was produced by replacing the luciferase gene of pGL3-*RGP* (37) with the *β-globin* intron from pCMV-neo-Bam3. pGL3-*RGP* contained a 5-kb *RGP* promoter (37). The transgene was excised as a MluI-AfeI fragment and was used to produce five transgenic lines in the C57BL/6J background; the intact transgene was confirmed by Southern blotting. *RGP-MDM2* mice were maintained by crossing to wild-type C57BL/6J mice and were PCR genotyped using forward primer 5′-CCTCTGCTAACCATGTTCATGCCT-3′ and reverse primer 5′-TCTTGTTCCGAAG-CTG-GAAT-3′ in the rabbit *β-globin* intron and MDM2 ORF, respectively. A third primer complementary to the murine (but not the human) *Mdm2 plus* strand (5′-CTCTCG-GATCACCGCGCTTCTCC-3′) was used as a PCR positive control.

Lentiviral shRNA and cDNA Constructs. pLKO shRNA vectors were obtained from the TRC library (Open Biosystems) or shRNA sequences were cloned into pLKO.1-YFP as described (27). The RSV promoter of pLKO.1 was replaced with the CMV promoter to produce pLKO.1C versions for enhanced virus production. We used pLKO.1C-YFP-sh*RB1*-733 (27) for human RB KD and pLKO.1C-YFP-sh*Rb1* [with targeting sequence 5′-AACGGACGTGTGAACTTA-TAT-3′ (40)] for mouse *Rb1* KD. pLKO.1C-YFP-sh*SCR* was based on Addgene plasmid 1864. The lentiviral cDNA expression vector BE-Neo (BN) was constructed as described (27). BN-*Mycn* had the mouse *Mycn* cDNA without UTRs between the BE-Neo MluI and XbaI sites. cDNA encoding stabilized Mycn^{T58A} was a gift from Gregory Shackelford, Children's Hospital Los Angeles, Los Angeles (54) and replaced wild-type *Mycn* using In-Fusion (Clontech).

Immunofluorescence Staining and Microscopy. Sections were air dried for ∼5 min and were washed with Tris-buffered saline (TBS) (Bioland Scientific LLC). All washes were with TBS. Sections were treated with EDTA (1 mM, pH 8.0) for 5 min at room temperature followed by blocking and permeabilization in super block

(27) for 1 h. Primary antibodies (*SI Appendix*, Table S1) were diluted in super block (27) overnight at 4 °C or 1 h at room temperature, followed by incubation with secondary antibodies for 30 min at room temperature. Sections were mounted in Mowiol (Calbiochem) with DABCO (Sigma). For quantitation of protein expression, $RXR\gamma^+$ or $ARR3^+$ cells were outlined and quantitated using ImageJ (55).

Statistical Analyses. For bivariate analysis of frequency data, Fisher's exact test was used. For multivariable analyses of mean Ki67 and EdU data (e.g., Fig. 4 *C*–*E*), ANOVA with Tukey's honestly significant difference (HSD) post hoc test was used. Other pairwise comparisons of mean percentage data were conducted using Student's *t* test as indicated.

ACKNOWLEDGMENTS. We thank Masayuki Akimoto and Anand Swaroop for *RGP-Cre* mice and pGL3-*RGP*; David MacPherson for $Rb1^{lox/lox}$ mice; Willie Marks for the production of *RGP-MDM2* mice; Esteban Fernandez for help with ImageJ; Ze'ev Ronai for pcDNA3-MDM2; Gregory Shackleford for $MYCN^{T58A}$ cDNA; Melissa L. Wilson (USC Department of Preventive Medicine and Family Planning Associates) for assistance in obtaining fetal tissue; David H. Abramson, Nai-Kong Cheung, and Thomas C. Lee for support; Jennifer Aparicio and Aaron Nagiel for critical reading of the manuscript; the Transgenic Mouse Core Facility of Memorial Sloan-Kettering Cancer Center; and the Stem Cell Analytics Core Facility, Animal Care Core Facility, and Imaging Core Facility of The Saban Research Institute of Children's Hospital Los Angeles. This study was supported in part by the Elsa U. Pardee Foundation, the Fund for Ophthalmic Knowledge, the Larry and Celia Moh Foundation, the Neonatal Blindness Research Fund, the A. B. Reins Foundation, a Young Investigator's Grant from Alex's Lemonade Stand Foundation (to S.L.), an unrestricted grant to the USC Department of Ophthalmology from Research to Prevent Blindness, and NIH Grants P30CA014089 and R01CA137124 (to D.C.).

1. Dimaras H, et al. (2015) Retinoblastoma. *Nat Rev Dis Primers* 1:15021.
2. Dimaras H, et al. (2008) Loss of RB1 induces non-proliferative retinoma: Increasing genomic instability correlates with progression to retinoblastoma. *Hum Mol Genet* 17:1363–1372.
3. Kooi IE, et al. (2016) Somatic genomic alterations in retinoblastoma beyond RB1 are rare and limited to copy number changes. *Sci Rep* 6:25264.
4. Zhang J, et al. (2012) A novel retinoblastoma therapy from genomic and epigenetic analyses. *Nature* 481:329–334.
5. Draper GJ, Sanders BM, Brownbill PA, Hawkins MM (1992) Patterns of risk of hereditary retinoblastoma and applications to genetic counselling. *Br J Cancer* 66:211–219.
6. Clarke AR, et al. (1992) Requirement for a functional Rb-1 gene in murine development. *Nature* 359:328–330.
7. Jacks T, et al. (1992) Effects of an Rb mutation in the mouse. *Nature* 359:295–300.
8. Lee EY, et al. (1992) Mice deficient for Rb are nonviable and show defects in neurogenesis and haematopoiesis. *Nature* 359:288–294.
9. Maandag EC, et al. (1994) Developmental rescue of an embryonic-lethal mutation in the retinoblastoma gene in chimeric mice. *EMBO J* 13:4260–4268.
10. Williams BO, et al. (1994) Extensive contribution of Rb-deficient cells to adult chimeric mice with limited histopathological consequences. *EMBO J* 13:4251–4259.
11. Chen D, et al. (2004) Cell-specific effects of RB or RB/p107 loss on retinal development implicate an intrinsically death-resistant cell-of-origin in retinoblastoma. *Cancer Cell* 5:539–551.
12. MacPherson D, et al. (2004) Cell type-specific effects of Rb deletion in the murine retina. *Genes Dev* 18:1681–1694.
13. Robanus-Maandag E, et al. (1998) p107 is a suppressor of retinoblastoma development in pRb-deficient mice. *Genes Dev* 12:1599–1609.
14. Zhang J, Schweers B, Dyer MA (2004) The first knockout mouse model of retinoblastoma. *Cell Cycle* 3:952–959.
15. Dannenberg JH, Schuijff L, Dekker M, van der Valk M, te Riele H (2004) Tissue-specific tumor suppressor activity of retinoblastoma gene homologs p107 and p130. *Genes Dev* 18:2952–2962.
16. MacPherson D, et al. (2007) Murine bilateral retinoblastoma exhibiting rapid-onset, metastatic progression and N-myc gene amplification. *EMBO J* 26:784–794.
17. Sangwan M, et al. (2012) Established and new mouse models reveal E2f1 and Cdk2 dependency of retinoblastoma, and expose effective strategies to block tumor initiation. *Oncogene* 31:5019–5028.
18. Wu N, et al. (2017) A mouse model of MYCN-driven retinoblastoma reveals MYCN-independent tumor reemergence. *J Clin Invest* 127:888–898.
19. Eagle RC, Jr (2013) The pathology of ocular cancer. *Eye (Lond)* 27:128–136.
20. Bogenmann E, Lochrie MA, Simon MI (1988) Cone cell-specific genes expressed in retinoblastoma. *Science* 240:76–78.
21. Gonzalez-Fernandez F, et al. (1992) Expression of developmentally defined retinal phenotypes in the histogenesis of retinoblastoma. *Am J Pathol* 141:363–375.
22. Nork TM, Schwartz TL, Doshi HM, Millecchia LL (1995) Retinoblastoma. Cell of origin. *Arch Ophthalmol* 113:791–802.
23. Rodrigues MM, et al. (1992) Retinoblastoma: Messenger RNA for interphotoreceptor retinoid binding protein. *Curr Eye Res* 11:425–433.
24. Xu XL, et al. (2009) Retinoblastoma has properties of a cone precursor tumor and depends upon cone-specific MDM2 signaling. *Cell* 137:1018–1031.
25. Ajioka I, et al. (2007) Differentiated horizontal interneurons clonally expand to form metastatic retinoblastoma in mice. *Cell* 131:378–390.
26. Bremner R, Sage J (2014) Cancer: The origin of human retinoblastoma. *Nature* 514:312–313.
27. Xu XL, et al. (2014) Rb suppresses human cone-precursor-derived retinoblastoma tumours. *Nature* 514:385–388.
28. Vooijs M, te Riele H, van der Valk M, Berns A (2002) Tumor formation in mice with somatic inactivation of the retinoblastoma gene in interphotoreceptor retinol binding protein-expressing cells. *Oncogene* 21:4635–4645.
29. Chen D, Chen Y, Forrest D, Bremner R (2013) E2f2 induces cone photoreceptor apoptosis independent of E2f1 and E2f3. *Cell Death Differ* 20:931–940.
30. Jin K, Xiang M (2012) In vitro explant culture and related protocols for the study of mouse retinal development. *Methods Mol Biol* 884:155–165.
31. Bull ND, et al. (2011) Use of an adult rat retinal explant model for screening of potential retinal ganglion cell neuroprotective therapies. *Invest Ophthalmol Vis Sci* 52:3309–3320.
32. Bumsted K, Jasoni C, Szél A, Hendrickson A (1997) Spatial and temporal expression of cone opsins during monkey retinal development. *J Comp Neurol* 378:117–134.
33. Young RW (1985) Cell differentiation in the retina of the mouse. *Anat Rec* 212:199–205.
34. Lee TC, Almeida D, Claros N, Abramson DH, Cobrinik D (2006) Cell cycle-specific and cell type-specific expression of Rb in the developing human retina. *Invest Ophthalmol Vis Sci* 47:5590–5598.
35. Mori M, Ghyselinck NB, Chambon P, Mark M (2001) Systematic immunolocalization of retinoid receptors in developing and adult mouse eyes. *Invest Ophthalmol Vis Sci* 42:1312–1318.
36. Sage J, Miller AL, Pérez-Mancera PA, Wysocki JM, Jacks T (2003) Acute mutation of retinoblastoma gene function is sufficient for cell cycle re-entry. *Nature* 424:223–228.
37. Akimoto M, et al. (2004) Transgenic mice expressing Cre-recombinase specifically in M- or S-cone photoreceptors. *Invest Ophthalmol Vis Sci* 45:42–47.
38. Fujieda H, Bremner R, Mears AJ, Sasaki H (2009) Retinoic acid receptor-related orphan receptor alpha regulates a subset of cone genes during mouse retinal development. *J Neurochem* 108:91–101.
39. Zhu X, et al. (2002) Mouse cone arrestin expression pattern: Light induced translocation in cone photoreceptors. *Mol Vis* 8:462–471.
40. Calo E, et al. (2010) Rb regulates fate choice and lineage commitment in vivo. *Nature* 466:1110–1114.
41. Carter-Dawson LD, LaVail MM (1979) Rods and cones in the mouse retina. II. Autoradiographic analysis of cell generation using tritiated thymidine. *J Comp Neurol* 188:263–272.
42. Qi DL, Cobrinik D (2017) MDM2 but not MDM4 promotes retinoblastoma cell proliferation through p53-independent regulation of MYCN translation. *Oncogene* 36:1760–1769.
43. Barak Y, Gottlieb E, Juven-Gershon T, Oren M (1994) Regulation of mdm2 expression by p53: Alternative promoters produce transcripts with nonidentical translation potential. *Genes Dev* 8:1739–1749.
44. Sears R, et al. (2000) Multiple Ras-dependent phosphorylation pathways regulate Myc protein stability. *Genes Dev* 14:2501–2514.
45. Sehgal R, Andres DJ, Adler R, Belecky-Adams TL (2006) Bone morphogenetic protein 7 increases chick photoreceptor outer segment initiation. *Invest Ophthalmol Vis Sci* 47:3625–3634.
46. Spencer C, et al. (2005) Distinct patterns of expression of the RB gene family in mouse and human retina. *Gene Expr Patterns* 5:687–694.
47. Welby E, et al. (2017) Isolation and comparative transcriptome analysis of human fetal and iPSC-derived cone photoreceptor cells. *Stem Cell Reports* 9:1898–1915.
48. O'Brien KM, Schulte D, Hendrickson AE (2003) Expression of photoreceptor-associated molecules during human fetal eye development. *Mol Vis* 9:401–409.
49. Cornish EE, Xiao M, Yang Z, Provis JM, Hendrickson AE (2004) The role of opsin expression and apoptosis in determination of cone types in human retina. *Exp Eye Res* 78:1143–1154.
50. Singh HP, Wang S, Cobrinik D (2016) Human cone precursor program underlying a proliferative response to pRB loss. *Invest Ophthalmol Vis Sci* 57:556.
51. Bourgo RJ, Ehmer U, Sage J, Knudsen ES (2011) RB deletion disrupts coordination between DNA replication licensing and mitotic entry in vivo. *Mol Biol Cell* 22:931–939.
52. Pettker CM, Goldberg JD, El-Sayed YY, Copel JA; Committee on Obstetric Practice, the American Institute of Ultrasound in Medicine, and the Society for Maternal-Fetal Medicine (2017) Committee opinion no 700: Methods for estimating the due date. *Obstet Gynecol* 129:e150–e154.
53. Cooper AR, et al. (2011) Highly efficient large-scale lentiviral vector concentration by tandem tangential flow filtration. *J Virol Methods* 177:1–9.
54. Shackleford GM, et al. (2016) BarTeL, a genetically versatile, bioluminescent and granule neuron precursor-targeted mouse model for medulloblastoma. *PLoS One* 11:e0156907.
55. Schneider CA, Rasband WS, Eliceiri KW (2012) NIH Image to ImageJ: 25 years of image analysis. *Nat Methods* 9:671–675.